Structural, electronic and catalytic properties of bimetallic Pt$_n$Ag$_n$ (n=1−7) clusters

P.L. Rodríguez-Kessler [a, *], A. Muñoz-Castro [a, **], P.A. Alonso-Dávila [b], F. Aguilera-Granja [c], A.R. Rodríguez-Domínguez [c, ***]

[a] Grupo de Química Inorgánica y Materiales Moleculares, Facultad de Ingeniería, Universidad Autónoma de Chile, El Llano Subercaseaux, 2810, Santiago, Chile
[b] Facultad de Ciencias Químicas, Universidad Autónoma de San Luis Potosí, San Luis Potosí, 78000, México
[c] Instituto de Física, Universidad Autónoma de San Luis Potosí, San Luis Potosí, 78000, México

ARTICLE INFO

ABSTRACT

The geometrical, electronic and catalytic properties of Pt$_n$Ag$_n$ (n = 1−7) clusters are investigated by means of density functional theory (DFT) computations. The ground state structures are obtained by a structure search procedure based in the simulated annealing method. In general, the Pt$_n$Ag$_n$ clusters adopt structures with Pt cluster motifs at the central position surrounded by silver islands. We found that the Pt$_4$Ag$_4$ and Pt$_6$Ag$_6$ clusters have a closed shell geometric structure and are the most stable clusters in this series. The bimetallic cluster reactivity is investigated by using the ionization potential, electron affinity, the d-band center, and the adsorption energy descriptors, respectively. However, it turns out that the reactivity of these systems is more sensitive to the chemical element on the cluster surface exhibiting a local reactivity. The different reactive sites on the cluster surface can be explained by the molecular electrostatic potential surface. In the Pt$_n$Ag$_n$ alloys, the Pt species perform similar interactions with a CO molecule in comparison to the unary Pt clusters, whereas the Ag species issue weaker interactions, increasing the catalyst resistance. In this context, the bimetallic clusters may serve as potential candidates for hydrogenation reactions. Furthermore, the distinct charge reorganization on the Pt$_n$Ag$_n$ alloys is useful for incorporating a lower number of noble metals in order to achieve an increased catalytic and selectivity capabilities. Theoretical data on the infrared spectra of the clusters is also provided.

© 2020 Elsevier B.V. All rights reserved.

1. Introduction

We are currently facing an accelerated global warming due to the accumulation of greenhouse gases in the atmosphere. To counteract this, an economy based on renewable energies is a potential approach to preserving the environment by reducing the carbon dioxide emissions [1−4]. Proton exchange membrane fuel cells (PEMFCs) are environmental-friendly which can replace the conventional fossil fuel-based engines in power transportation vehicles. Platinum nanoparticles dispersed in amorphous carbon materials (Pt/C) are standard catalysts for the oxygen reduction reaction ORR, which is the principal reaction in PEMFCs [5,6]. However the high cost and poor long-term stability of Pt/C catalysts make this technology inaccessible for commercialization. Compared with pure Pt bulk catalysts, the Pt-TM alloys compounded with transition metal (TM) elements in the *3d* block (TM = Co, Ni, Fe, etc.) exhibit better catalytic activity and lower cost [7−11]. However, the electrochemical stability of Pt-TM alloy NPs is still under debate. The tendency to dissolve in acidic solutions is attributed to the relatively low cohesive energy of Pt alloy NPs [12−14]. Thus, raising the cohesive energy of Pt-based alloy NPs will improve their stability [15−17]. On the other hand, bimetallic noble metal clusters have attracted significant interest since they can be favorable for the ORR [14]. Yancey et al. synthesized Au@Pt dendrimer-encapsulated nanoparticles and discovered that Au$_{147}$@Pt exhibited higher ORR activity than Au and Pt nanoparticles alone [18]. Harada et al. conducted electrocatalytic tests on Pt−Au clusters and found a significant increase in ORR rate after Pd deposition [19]. In addition, there are also several specific

* Corresponding author.
** Corresponding author.
*** Corresponding author.
E-mail addresses: rodriguezkessler.p@gmail.com (P.L. Rodríguez-Kessler), alvaro.munoz@uautonoma.cl (A. Muñoz-Castro), adnrdz@ifisica.uaslp.mx (A.R. Rodríguez-Domínguez).
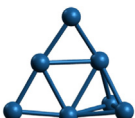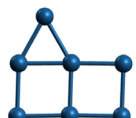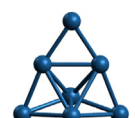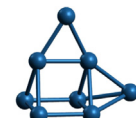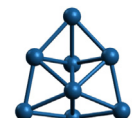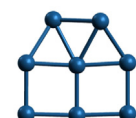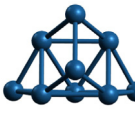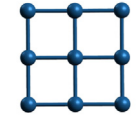
challenges for different noble metal clusters and the alloyed clusters. For noble metal clusters, because of the ultra-high price, it is still necessary to reduce the size of the particles, in order to reduce the costs. Experimentally, various bimetallic nanoparticles have been synthesized by using dendrimer templates [20]. Combinations using Au, Pd, and Pt elements have been reported in a number of theoretical and experimental works, and the catalytic activities have been investigated. Crooks et al. synthesized bimetallic PdAu dendrimer-encapsulated catalysts and found improved catalytic activities of the hydrogenation of allyl alcohols in the presence of the alloy and core/shell PdAu nanoparticles as compared to single metals [21]. Experimental studies on the catalytic activity of Au−Pt alloy nanoparticl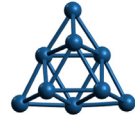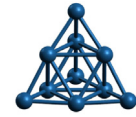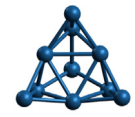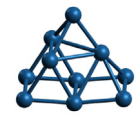es have been found excellent catalytic performance for CO oxidation [22]. Hydrogenation reactions on Au-core Pt-shell bimetallic nanoparticles showed greater activity than Pt nanoparticles and a physical mixture of Pt and Au nanoparticles. These results suggest that the presence of electron deficient platinum is caused by the Au core [23]. On the other hand, Pd−Ag bimetallic nanoparticles were synthesized at three different Pd:Ag ratios. Increasing the Ag:Pd ratio provided a core-shell structure where Ag dominates the outer shell. The catalytic activity was investigated and indicated that the Ag content improves selectivity for alkyne hydrogenation [24]. However, as the best to our knowledge, the synthesis of Pt−Ag bimetallic clusters and their catalytic activities have not been explored so far. Motivated by the above and the extensive applications of Pt-M alloy catalysts, in the following, we present a systematic calculation on the structure, electronic and magnetic properties of Pt_nAg_n ($n = 1-7$) clusters. The results show that the Pt_nAg_n bimetallic clusters have less reduction ability compared to the unary clusters, however, due to the closed shell geometrical arrangement on Pt_6Ag_6, more CO tolerance is found which may serve as potential systems for hydrogenation reactions. The structural and electronic properties of these clusters are discussed in detail.

2. Computational details

The calculations in this work are based on the framework of spin-polarized density functional theory (DFT) [25,26] implemented in the Vienna *ab initio* simulation package (VASP) [27,28], which solves the Kohn-Sham equations under periodic conditions by using a plane wave (PW) basis set. The interactions between the ions and valence electrons are described by the projector augmented-wave (PAW) method [29]. The exchange correlation (XC) functional is treated using the PBE approximation [30]. The wave functions are expanded in plane-wave basis sets with a cutoff energy of 400 eV. The atomic positions are relaxed self-consistently by the conjugate gradient method algorithm until the forces are smaller than 0.01 eV/Å for all atoms. We used a cubic box with a size of 16 Å for geometry calculations, which is large enough to avoid the interaction between periodic images. Due to the size of the supercell, only the Γ point is taken into account to represent the Brillouin zone. The lowest energy structures of Pt_nAg_n clusters are determined by Simulated annealing (SA) based on *ab initio* molecular dynamics (AIMD) in the basis of the NVT ensemble with the Nosé-Hoover approach, as implemented in the VASP code. Temperature is increased rapidly up to 2000 K and lowered gradually to 0 K, with a time step of 10 fs during 30 ps. The lowest energy configurations obtained by the AIMD-SA procedure, are further calculated with the conjugate-gradient algorithm in different values of the total spin magnetic moment. The most stable structures are corroborated by additional AIMD-SA runs by using different initial structures. Finally, the vibrational spectra of the clusters are calculated by using the Gaussian09 [31] program. The PW91 exchange-correlation functional [32] and the cc-pVDZ-PP basis set are used, in which PP means for a pseudopotential [33]. The interactions between the valence electrons and the inert core are included in the pseudopotential, which also includes the relativistic effects of heavy elements. The accuracy of this computational approach when predicting molecular geometries, vibrational spectra, and some thermodynamic parameters for silver clusters has been demonstrated in literature [34,35].

Table 1
Ground-state structures and low-lying isomers of Pt_n ($n = 7-10$) clusters. For each cluster, the average binding energy (E_B) including SOC is given in parentheses. Distances are given in Å.

Notation	Pt_7^A	Pt_7^B	Pt_7^C	Pt_8^A	Pt_8^B	Pt_8^C
Structure						
E_B(eV/atom)	3.28 (3.17)	3.25 (3.16)	3.25 (3.17)	3.39 (3.21)	3.38 (3.23)	3.36 (3.21)
$\mu(\mu_B)$	4.00	4.00	6.00	0.00	2.00	2.00
Bond length (Å)	2.44 - 2.74	2.43 - 2.50	2.48 - 2.73	2.47 - 2.61	2.51 - 2.99	2.41 - 2.58

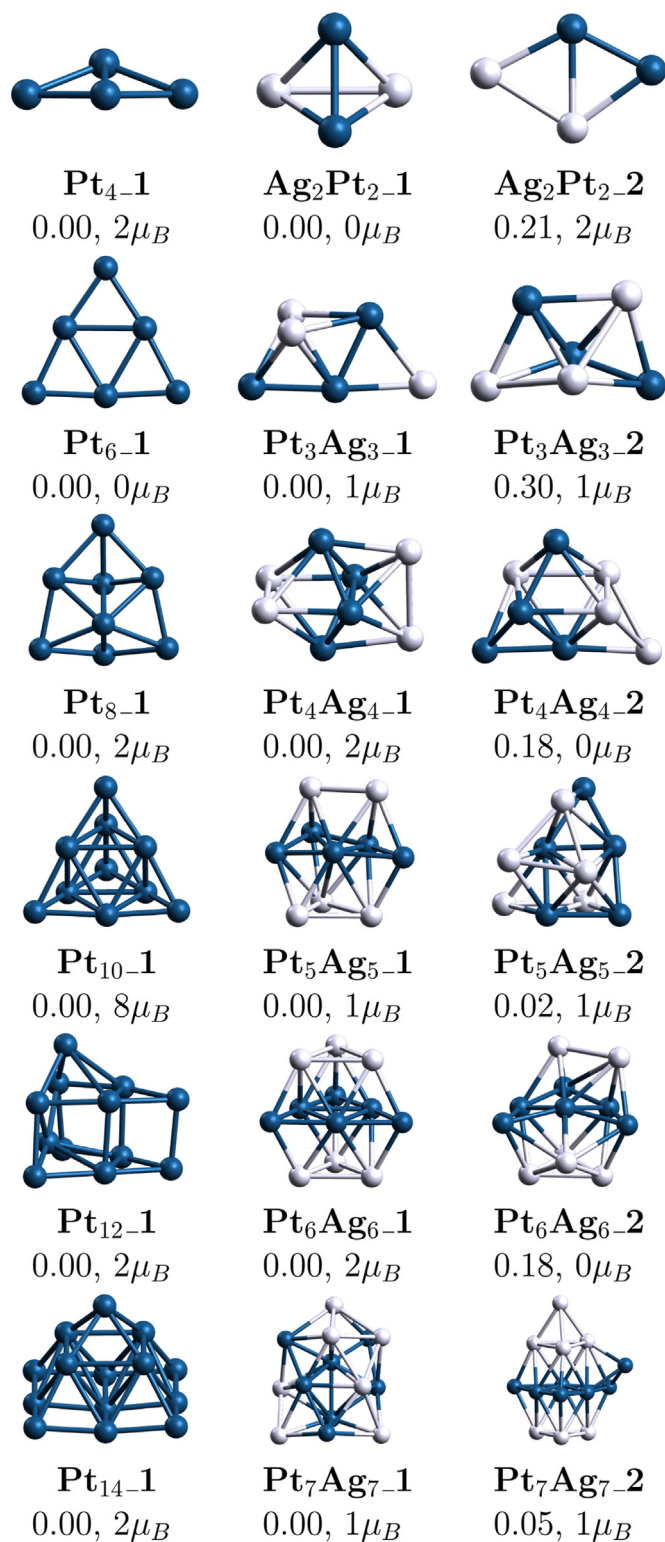| Notation	Pt_9^A	Pt_9^B	Pt_9^C	Pt_{10}^A	Pt_{10}^B	Pt_{10}^C
Structure						
E_B(eV/atom)	3.52 (3.36)	3.52 (3.35)	3.50 (3.35)	3.67 (3.52)	3.65 (3.49)	3.55 (3.41)
$\mu(\mu_B)$	6.00	4.00	8.00	8.00	2.00	4.00
Bond length (Å)	2.51 - 2.77	2.45	2.55 - 2.76	2.54 - 2.76	2.52 - 2.74	2.53 - 2.97

Fig. 1. Lowest energy structures of Pt_nAg_n and Pt_{2n} clusters (with $n = 2-7$) calculated by using PBE in VASP.

bond length of the Pt_2 dimer is 2.32 Å and magnetic moment of $2\mu_B$, which is found in good agreement with respect to experimental and theoretical values. A comparison of these parameters with a number of works is available elsewhere [36]. Although the PW91 functional offers a Pt–Pt bond closer to the experiment, the binding energy is slightly larger. In calculations reported by Huda et al. [37] the inclusion of the spin orbit coupling (SOC) shows a reduction of the binding energy, leading to a closer value to the experimental one [38]. Blonski et al. [39], determined that the SOC plays an important role in determining the geometric structure of Pt clusters. Since the structures of Pt_n are crucial to determine their catalytic properties, in our recent work we found that the SOC effect stabilizes the structures of Pt_n clusters up to 13 atoms [36]. We have not discussed the structures of Pt_n ($n = 7-10$) clusters so far, this series of clusters will be useful for comparing our present results on the bimetallic ones. Our spin polarized calculations without restrictions in the geometry for these clusters with the first low lying isomers (denoted with letters A,B,C, etc, ordered decreasing its stability without SOC.) are shown in Table 1. For Pt_7, semiplanar structures are found as the most stable configurations. By including the SOC effect, the Pt_7^A and Pt_7^C structure become more comparative in stability. For Pt_8 we found a cluster formed by a triangular prism capped in two different sites. Including the relativistic effects, a triple tetragonal pyramid (TTB) with $2\mu_B$ becomes the more stable one. The Pt_8^B structure has been suggested as the global minimum for Pt_8, and a comparative study on the stability on Pt_8 was reported by Sebetci [40]. The most stable structure for Pt_9^B is a three-dimensional structure, followed by a planar one. Pt_{10} is a tetrahedron or triangular pyramid. In the size range of $n = 11-14$ atoms, Pt_n clusters display a preference for layered and pyramidal geometries [41]. The lowest energy structure of Pt_{12} is shown in Fig. 1 and is used for comparison. A more detailed discussion about the Pt_{12} cluster structure isomers can be found in our previous work [36]. Pt_{14} adopts a pyramidal structure, which is in well agreement with recent reports [41,42]. Finally, as pointed out before in this work, we use the results of Pt_{2n} ($n = 1-7$) as a reference to see the alloy effects in the case of the bimetallic system, mainly concern to the electronic properties.

3.2. Structural behavior of bimetallic Pt_nAg_n clusters

The PtAg dimer is double state with a bond length of 2.52 Å. In regard to the most stable forms of the Pt_nAg_n alloys, it can be observed that the Pt atoms remain always together in the central position of the clusters while Ag form islands on the surface sites. The most stable structure for Pt_2Ag_2 is a tetrahedron, while a planar rhombus is 0.21 eV higher in energy (see Fig. 1). However by setting the SOC, ΔE becomes only 0.03 eV, suggesting that both structures can occur in real conditions. The most stable structures for Pt_3Ag_3 are formed by a trigonal bipyramid (TBP) motif with the addition of an Ag atom in the bridge site (lowest) and the hollow site (next isomer) with $\Delta E = 0.30$ (0.07) eV, respectively. The lowest energy structure for Pt_4Ag_4 is a bicapped octahedron. By inspection of Pt_4Ag_4, we noticed that it can be formed by a bent rhombus (lowest energy structure for Pt_4) located in the central position, surrounded by extra Ag atoms binding to the face sites of Pt_4. In this context, Pt_5Ag_5 is also formed by the Pt_5 lowest energy structure (side capped square) sandwiched by Ag islands. Pt_6Ag_6 is a hcp-like structure, formed by a planar triangle (Pt_6 most stable cluster) sandwiched by two Ag_3 triangles. The lowest energy structure for Pt_7Ag_7 is a bilayered structure. Interestingly these structures are found stable for other metallic species such as Pd_{13} [43,44]. The Pt atoms in Pt_7Ag_7 also form a stable isomer for Pt_7, but not necessarily the most stable one. According to these observations the structure
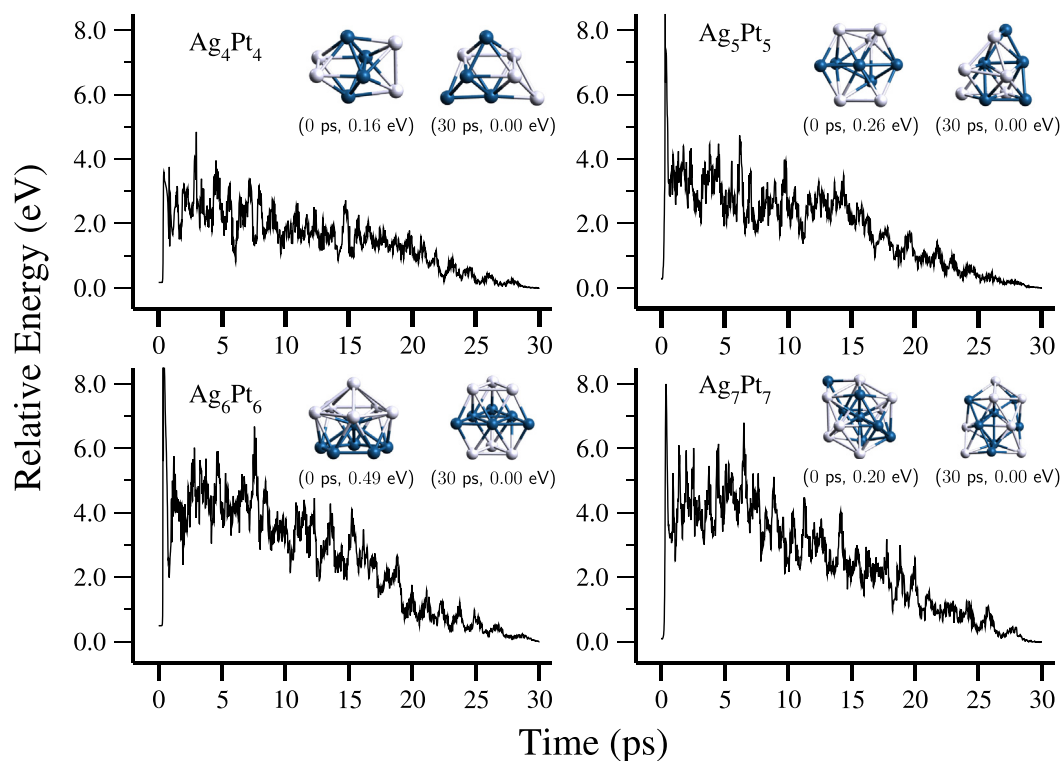
3. Results and discussion

3.1. Brief review on Pt_n clusters

According to our computational details described above, the

Fig. 2. AIMD-SA calculations on Pt_nAg_n ($n = 4-7$) clusters. The elapsed time during simulation and relative energy for the initial and final configurations are shown.
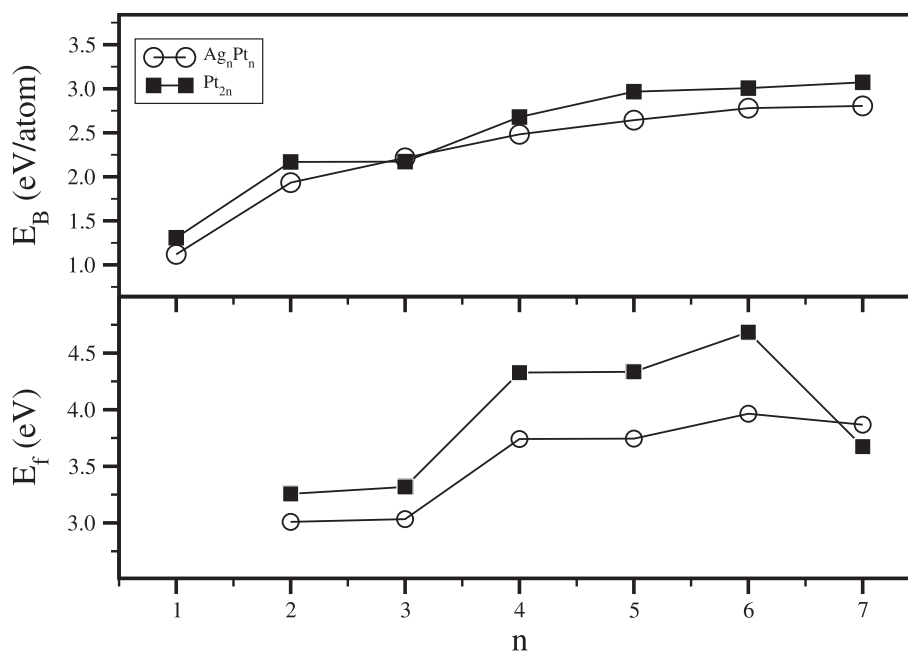

Fig. 3. Average binding energy and fragmentation energy of Pt_nAg_n ($n = 1-7$) clusters as a function of size.

for larger Pt_nAg_n clusters can be predicted by decorating stable Pt_n isomers with Ag islands. However, due to the problem complexity, it is also important to confirm the results with efficient structure searches. In Fig. 2, the AIMD simulations for Pt_nAg_n (n = 4−7) clusters are displayed, showing a viable strategy for the structural prediction of the alloy clusters.

3.3. Electronic properties

The stability of Pt_nAg_n clusters is further investigated by calculating the binding energy per atom (E_B), and fragmentation energy (E_f) parameters. The results are shown in Fig. 3, while definitions are in the Supplementary data (page S2) available. The results of the average binding energy (E_B) show that the bimetallic Pt_nAg_n clusters have slightly lower binding energies, suggesting that the Pt−Ag
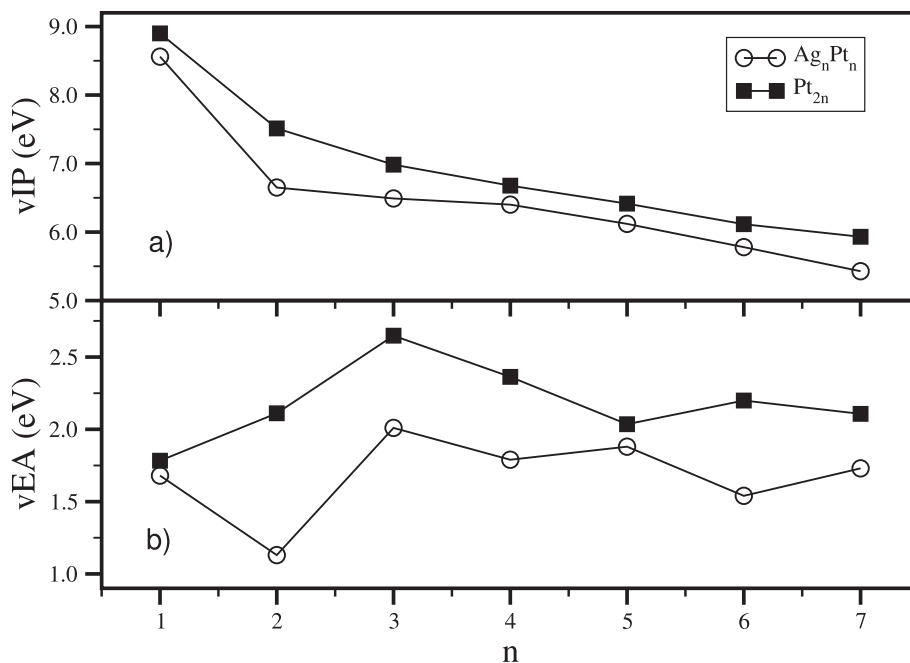
Fig. 4. The vIP and vEA values of Pt_nAg_n (open figures) and Pd_{2n} (closed figures) clusters.

Table 2
The vIP and vEA parameters for the Pt_nAg_n and Pt_n clusters. The spin-resolved d-band center (ε_d) for the clusters is also provided.

n	vIP (eV)		vEA (eV)		$\varepsilon_{d\uparrow}$ (eV)		$\varepsilon_{d\downarrow}$ (eV)	
	Pt_nAg_n	Pt_{2n}	Pt_nAg_n	Pt_{2n}	Pt_nAg_n	Pt_{2n}	Pt_nAg_n	Pt_{2n}
1	8.56	(8.90)	1.68	(1.78)	−1.80	(−1.63)	−1.53	(−0.98)
2	6.65	(7.51)	1.13	(2.11)	−2.20	(−1.65)	−2.20	(−1.33)
3	6.49	(6.98)	2.01	(2.64)	−2.26	(−1.64)	−2.17	(−1.64)
4	6.40	(6.67)	1.79	(2.36)	−2.45	(−1.86)	−2.31	(−1.71)
5	6.12	(6.41)	1.88	(2.03)	−2.48	(−2.09)	−2.44	(−1.62)
6	5.78	(6.11)	1.54	(2.19)	−2.61	(−2.12)	−2.51	(−2.02)
7	5.42	(5.93)	1.73	(2.10)	−2.65	(−2.03)	−2.61	(−1.94)

bond is weaker the Pt−Pt one.

In general, there is an increase in the binding energy as a function of the cluster size for Pt_nAg_n ($n = 6-7$) clusters. The fragmentation energy (E_f) helps us to determine the relative stability of Pt_nAg_n clusters compared with their neighbors. For E_f, small odd-even oscillations are shown with the maximum values at Pt_4Ag_4 and Pt_6Ag_6. We attribute these maximal values due to the closed geometric structure as well as the chemical ordering that show partial mixing with central segregation. The maximal value of E_f corresponds to Pt_6Ag_6, suggesting that the later possesses enhanced stability. The increased stability of the Pt_6Ag_6 cluster can be understood by its symmetric arrangement.

To further analyze the electronic stability of the clusters we have calculated the vertical ionization potential (vIP) and the vertical electron affinity (vEA) parameters. The equations and definitions are provided in the Suppl. data (page S2) and also can be found elsewhere [45]. The variation of the vIP and vEA parameters as a function of the cluster size are shown in Fig. 4 and tabulated in Table 2. For both the bimetallic alloys and the unary Pt clusters, the vIP parameters show a decrease as the cluster size increases, which is consistent with the increment of electrons in the system. For vEA, the calculated values show more variation with respect to the cluster size. The values for vEA are smaller compared to the unary Pt clusters, which suggest that the bare ones have more ability for

reduction reactions [46].

By analyzing the electronic structure on the clusters, the results on the density of states (see Fig. 5) show that Pt_nAg_n clusters are weakly magnetic, as expected in regard to the unary Pt clusters. Pt_nAg_n clusters with $n = 4$ and 6 have $2\mu_B$ of total magnetic moment, while the remaining clusters in this series have 1 or $0\mu_B$ of magnetic moment. We have included the results on the unary Pt clusters of each size for comparison. Since most of unary Pt clusters are magnetic, we show the spin resolved density of states obtained from Gaussian broadening (half width of 0.05 eV) of the energy levels. Detailed studies on the electronic properties of Pt clusters are available elsewhere [42]. The spectra of the clusters show sharp peaks due to the relatively open structures of the clusters. For the unary Pt_{2n} clusters, there appears discrete peaks on $n = 3$ and $n = 5$, which corresponds to the planar triangle (Pt_6) and the tetrahedral (Pt_{10}) structure. While for the bimetallic alloy, discrete peaks are found only in Pt_6Ag_6 due to the symmetric structure. As the size of the clusters increases, we can also find more states near the Fermi energy level suggesting the metallic behavior on these systems. Such states near the Fermi level are consistent with the small HOMO-LUMO gaps (Δ_{H-L}) reported on Pt_n clusters [41]. There are isolated cases in which we can appreciate a large Δ_{H-L} value but only in one spin component. In order to analyze the chemical stability of these systems, we have determined the chemical hardness (η), which can be derived from the vIP and vEA values. The definition of η is available in page S3, and more details are available elsewhere [47,48]. We found that η decreases monotonically as a function of the cluster size, suggesting that the larger clusters exhibit a metallic-like electronic structure (see Fig. 6). We further have calculated the d-band center of the clusters which is an important parameter to determine the reactivity of clusters and surfaces. More details about this parameter are available in page S3, as well as in the following literature [36]. In general, it turns out that the bimetallic clusters have lower values on d_ε, suggesting that the bimetallic clusters may be less reactive (in average) than the unary ones, which is consistent with the vEA parameter. However, from the inspection of the electronic parameters discussed above, the reactivity of these systems is not very sensitive to the cluster
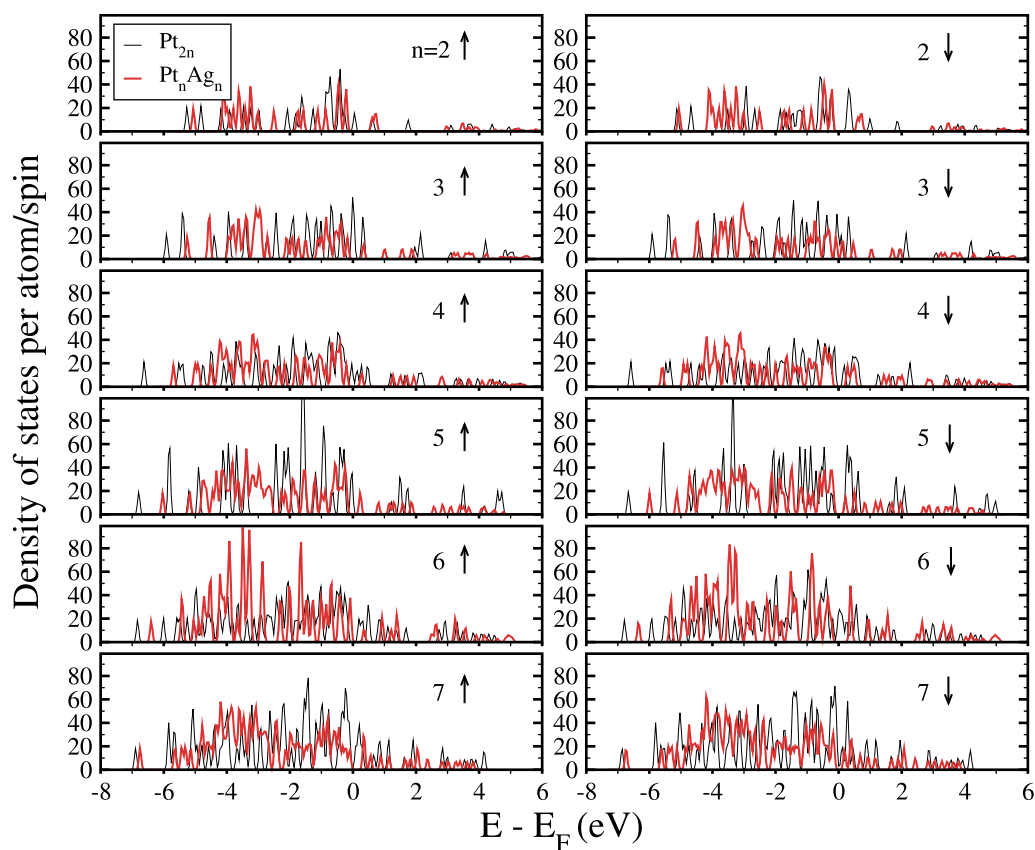
Fig. 5. The total density of states of Pt_nAg_n (red lines) and Pt_{2n} (black lines) clusters with $n = 1-7$, obtained by using PBE in VASP are presented. The Fermi level was taken as the zero of energy. (For interpretation of the references to colour in this figure legend, the reader is referred to the Web version of this article.)
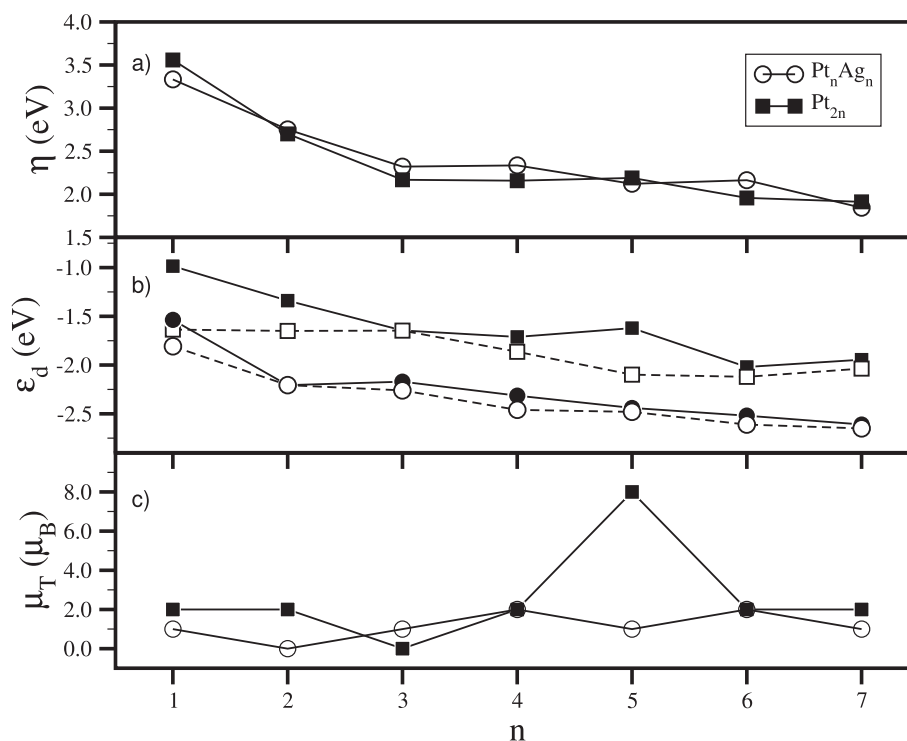

Fig. 6. The chemical hardness (η) of Pt_{2n} and Pt_nAg_n ($n = 1-7$) clusters obtained with PBE in VASP, respectively. The spin resolved d-band center (ε_d) of the clusters is also shown. The open figures correspond to the mayority spin ($\varepsilon_{d\uparrow}$) while the closed ones to the minority spin ($\varepsilon_{d\downarrow}$) parameters.
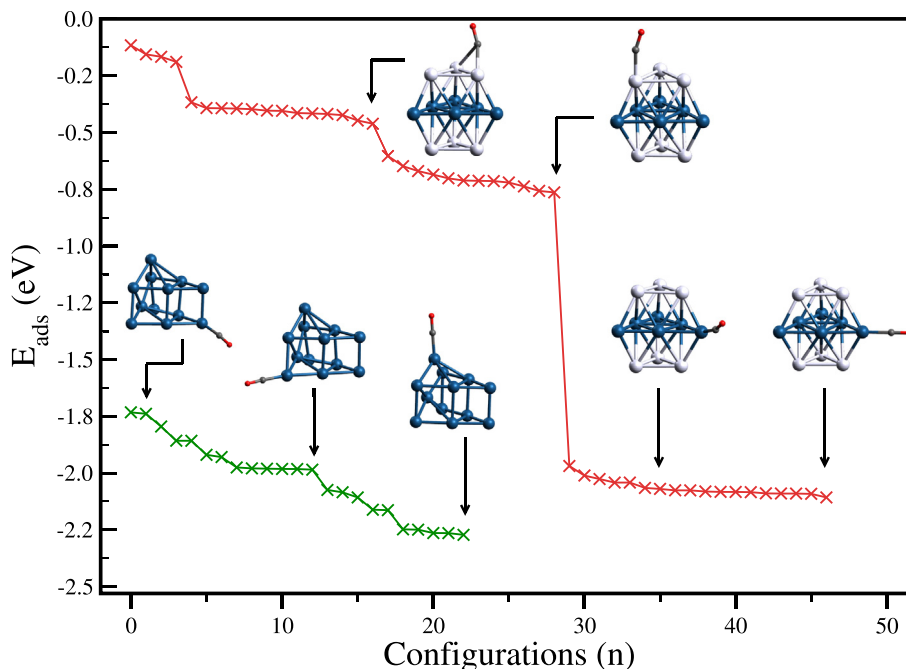
Fig. 7. Adsorption energy as a function of atomic configurations for CO on Pt$_6$Ag$_6$ and Pt$_{12}$ clusters.

size. For example, strong size dependent reactivity properties have been found for Ni$_n$ clusters [49,50]. Thus, we further analyze the reactivity on the clusters by exploring the interaction of a CO molecule on the cluster surface.

3.4. CO adsorption

In accordance to the results analyzed above, we further investigate whether the bimetallic clusters could have more tolerance toward CO poisoning in comparison to the unary ones. We have explored the CO adsorption on the Pt$_6$Ag$_6$ and Pt$_{12}$ clusters in order to determine the most reactive sites. The adsorption energy of the clusters has been determined after exploring a large number of adsorption configurations using the methodology explained in our previous work [49]. As we expected, the strongest reactivity on the clusters is taking place at the border sites (see Fig. 7). On the Pt$_6$Ag$_6$ bimetallic cluster, the adsorption energy values on the Pt sites are quite similar (with $E_{ads} \approx -2.0$ eV) than those of the unary Pt$_{12}$ cluster. It is important to note that the CO molecule can be adsorbed at different angles, showing similar interactions on the cluster surface. On the other hand, in the Pt$_n$Ag$_n$ alloy, the reactivity on the Ag atoms is drastically smaller (with $E_{ads} \leq -0.8$ eV). According to this, the reactivity is kind sensitive to the geometric position of the chemical species (for example, Ag atoms on the cluster surface). This result can also be explained by the electrostatic potential map, as shown in Fig. 8. Such analysis can be useful to determine the reactivity of other Pt bimetallic alloys.

The electrostatic potential surfaces have been shown to be useful to characterize catalytic sites on metallic clusters [51]. Particularly, for platinum clusters, the active sites are denoted by positive values of the potential, which are larger in magnitude than the observed for related gold clusters [51]. For Pt$_{12}$, the most positive region is located at platinum corners, as discussed above, with a small presence from the edge sites. This is given by the low-coordination number at the Pt corners resulting in a depletion of charge towards Pt–Pt bonding region within the cluster. Interestingly, for Pt$_6$Ag$_6$, the positive charge now is located at corners from

the equatorial Pt$_6$ region, suggesting the enhance in the catalytic activity in comparison to Pt$_{12}$, resulting, accounting for more favorable adsorption energy calculated above. In this sense, the isolation and enhance of the active catalytic sites can be obtained by the consecutive doping of monometallic clusters. Such an approach is useful for further rationalization of small cluster catalysts, which can incorporate a lower number of noble metals, in order to achieve an increased catalytic and selectivity capabilities.

Recently, the graphene nanosheet has been extensively investigated in electrode materials of proton exchange membrane fuel cells [52]. It has been shown that the equilibrium structures of the gas-phase Pt and Pt-alloy clusters are preserved if they are
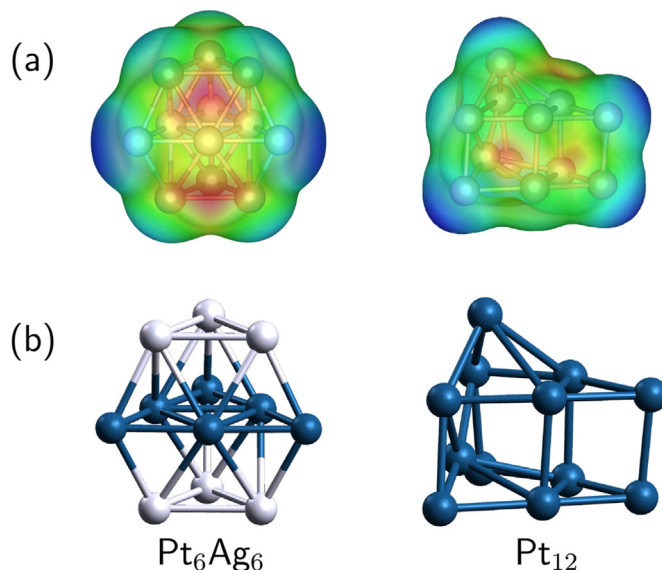

Fig. 8. Electrostatic potential superimposed on electron density maps (a) and structures (b) of Pt$_6$Ag$_6$ and Pt$_{12}$ clusters.
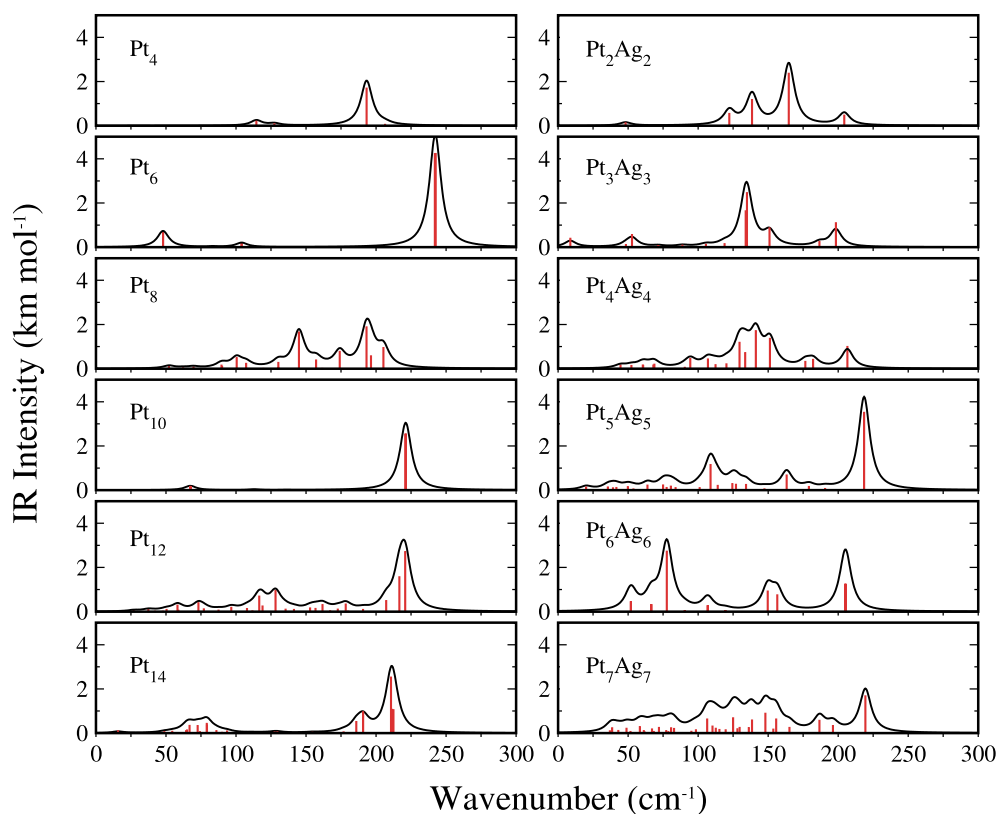
Fig. 9. Infrared Spectra of Pt_{2n} (left) and Pt_nAg_n (right) clusters with $n = 2-7$, obtained by using the PW91/cc-pVDZ-PP level with the GAUSSIAN G09 program.

deposited on graphene [39,53]. It is thus of fundamental importance the assignment of the most stable structures and electronic properties of PtAg alloys. The present results allow us to shed some light on the understanding of the catalytic behavior of these alloy clusters which are prospects for further research in catalysis.

3.5. Infrared Spectra of Pt_nAg_n (n = 1–7) clusters

The IR spectrum of the clusters provide useful information which may serve as a guide for experimental studies. In what follows we present the results on the IR spectra of the clusters, which are shown in Fig. 9. These spectra have been obtained by using the PW91/cc-pVDZ-PP level with the GAUSSIAN G09 program. The vibrational frequency of Pt_2 is $\omega = 233.8\ cm^{-1}$, which is in good agreement with experimental ($\omega = 217.20\ cm^{-1}$) [54] and theoretical studies [55]. For Pt_{2n} (with $n = 2$), the vibrational modes are found at 27.8, 114.5, 127.4, 146.4, 193.2, and 206.4 cm^{-1}. The lowest vibrational frequencies for Pt_{2n} ($n = 3-7$) are found at 40.6, 46.1, 47.8, 26.9, and 15.7 cm^{-1}, and the highest vibrational frequencies are found at 242.6, 205.2, 221.2, 220.7 and 216.7 cm^{-1}, respectively.

The harmonic frequency for the PtAg dimer is 189.7 cm^{-1}, which is associated with the Pt–Ag stretching mode. The highest intensity IR modes in Fe_2Pt_2 are 164.7 and 204.3 cm^{-1}, respectively, which are lower compared to the Pt_4 unary cluster. The lowest vibrational frequencies for Pt_3Ag_3, Pt_4Ag_4, Pt_5Ag_5, Pt_6Ag_6, and Pt_7Ag_7 are found at 8.7, 44.5, 20.0, 41.7, and 37.0 cm^{-1}, while the highest vibrational frequencies are found at 198.3, 206.6, 218.5, 205.2, and 219.4 cm^{-1} respectively. We associate the highest peak on Pt_6Ag_6 (with 205.2 cm^{-1}) can be related to the Pt_6 fragment (with 242.6 cm^{-1}) which have a red shift due to the Ag atoms in the alloy. For a given bimetallic cluster, the Pt–Ag stretching modes can be associated with lower frequency IR modes, which is consistent to the weaker

Pt–Ag bond. The structures of PtAg exhibit the highest IR intensity modes due more homogeneous Pt–Pt bonds than in other compositions for a given cluster.

4. Conclusions

In the present work, the structural, electronic and catalytic properties of Pt_nAg_n ($n = 1-7$) clusters are investigated by means of density functional theory (DFT) computations. The lowest energy structures and first low-lying isomers of these clusters were identified by a structure search procedure based in simulated annealing within the Nosé-Hoover thermostat. The results show that the reactivity of the clusters is more sensitive to the chemical species than to their electronic properties. We found that the Pt_4Ag_4 and Pt_6Ag_6 clusters possess a closed shell geometric structure and are the most stable in this series. In the Pt_nAg_n alloys, the Pt species perform similar interactions with a CO molecule in comparison to the unary Pt clusters, whereas the Ag species perform lower interactions, increasing the CO tolerance. In this context, the bimetallic clusters may serve as potential candidates for hydrogenation reactions. Furthermore, the distinct charge reorganization on the Pt_nAg_n alloys is useful for incorporate a lower number of noble metals in order to achieve an increased catalytic and selectivity capability. The data provided in this work can serve as a guide to further confirm the catalytic activity of the clusters experimentally.

Declaration of competing interest

The authors declare that they have no known competing financial interests or personal relationships that could have appeared to influence the work reported in this paper.

Acknowledgement

Appendix A. Supplementary data

Supplementary data to this article can be found online at https://doi.org/10.1016/j.jallcom.2020.155897.

References

[1] J.A. Turner, Sustainable hydrogen production, Science 305 (2004) 972−974.
[2] S. Chu, A. Majumdar, Opportunities and challenges for a sustainable energy future, Nature 488 (2012) 294−303.
[3] N.S. Lewis, D.G. Nocera, Powering the planet: chemical challenges in solar energy utilization, Proc. Natl. Acad. Sci. Unit. States Am. 103 (2006) 15729−15735.
[4] Z.W. She, J. Kibsgaard, C.F. Dickens, I. Chorkendorff, J.K. Nørskov, T.F. Jaramillo, Combining theory and experiment in electrocatalysis: insights into materials design, Science 355 (2017).
[5] J.K. Nørskov, J. Rossmeisl, A. Logadottir, L. Lindqvist, J.R. Kitchin, T. Bligaard, H. Jónsson, Origin of the overpotential for oxygen reduction at a fuel-cell cathode, J. Phys. Chem. B 108 (2004) 17886−17892.
[6] W. Reitz, Handbook of fuel cells: fundamentals, technology, and applications, (volume 2), in: W. Vielstich, A. Lamm, H.A. Gasteiger (Eds.), Mater. Manuf. Process, vol. 22, 2007, 789−789.
[7] K.J.J. Mayrhofer, B.B. Blizanac, M. Arenz, V.R. Stamenkovic, P.N. Ross, N.M. Markovic, The impact of geometric and surface electronic properties of Pt-catalysts on the particle size effect in electrocatalysis, J. Phys. Chem. B 109 (2005) 14433−14440.
[8] B.C. Han, C.R. Miranda, G. Ceder, Effect of particle size and surface structure on adsorption of O and OH on platinum nanoparticles: a first-principles study, Phys. Rev. B 77 (2008), 075410.
[9] M. Avramov-Ivic, R. Adzic, A. Bewick, M. Razaq, An investigation of the oxidation of formaldehyde on noble metal electrodes in alkaline solutions by electrochemically modulated infrared spectroscopy (emirs), J. Electroanal. Chem. 240 (1988) 161−169.
[10] V.R. Stamenkovic, B.S. Mun, M. Arenz, K.J.J. Mayrhofer, C.A. Lucas, G. Wang, P.N. Ross, N.M. Markovic, Trends in electrocatalysis on extended and nanoscale Pt-bimetallic alloy surfaces, Nat. Mater. 6 (2007) 241−247.
[11] L. Xiong, A. Kannan, A. Manthiram, Pt-M (M=Fe, Co, Ni and Cu) electrocatalysts synthesized by an aqueous route for proton exchange membrane fuel cells, electrochem, Commun. Now. 4 (2002) 898−903.
[12] R. Jinnouchi, E. Toyoda, T. Hatanaka, Y. Morimoto, First principles calculations on site-dependent dissolution potentials of supported and unsupported Pt particles, J. Phys. Chem. C 114 (2010) 17557−17568.
[13] E. Antolini, J.R. Salgado, E.R. Gonzalez, The stability of Pt-M (M=first row transition metal) alloy catalysts and its effect on the activity in low temperature fuel cells: a literature review and tests on a Pt-Co catalyst, J. Power Sources 160 (2006) 957−968.
[14] L. Tang, B. Han, K. Persson, C. Friesen, T. He, K. Sieradzki, G. Ceder, Electrochemical stability of nanometer-scale Pt particles in acidic environments, J. Am. Chem. Soc. 132 (2010) 596−600.
[15] M.J. Piotrowski, P. Piquini, J.L. Da Silva, Platinum-based nanoalloys $Pt_nTM_{55−n}$ (TM = Co, Rh, Au): a density functional theory investigation, J. Phys. Chem. C 116 (2012) 18432−18439.
[16] S.H. Noh, M.H. Seo, J.K. Seo, P. Fischer, B. Han, First principles computational study on the electrochemical stability of Pt-Co nanocatalysts, Nanoscale 5 (2013) 8625−8633.
[17] D. Guedes-Sobrinho, R.K. Nomiyama, A.S. Chaves, M.J. Piotrowski, J.L.F. Da Silva, Structure, electronic, and magnetic properties of binary $Pt_nTM_{55−n}$ (TM = Fe, Co, Ni, Cu, Zn) nanoclusters: a density functional theory investigation, J. Phys. Chem. C 119 (2015) 15669−15679.
[18] D.F. Yancey, E.V. Carino, R.M. Crooks, Electrochemical synthesis and electrocatalytic properties of Au@Pt dendrimer-encapsulated nanoparticles, J. Am. Chem. Soc. 132 (2010) 10988−10989.
[19] M. Harada, H. Noguchi, N. Zanetakis, S. Takakusagi, W. Song, K. Uosaki, Construction of multilayers of bare and Pd modified gold nanoclusters and their electrocatalytic properties for oxygen reduction, Sci. Technol. Adv. Mater. 12 (2011), 044606.
[20] K. Yamamoto, T. Imaoka, M. Tanabe, T. Kambe, New horizon of nanoparticle and cluster catalysis with dendrimers, Chem. Rev. 120 (2020) 1397−1437.
[21] R.W.J. Scott, O.M. Wilson, S.-K. Oh, E.A. Kenik, R.M. Crooks, Bimetallic palladium-gold dendrimer-encapsulated catalysts, J. Am. Chem. Soc. 126 (2004) 15583−15591.
[22] B.J. Auten, H. Lang, B.D. Chandler, Dendrimer templates for heterogeneous catalysts: bimetallic Pt-Au nanoparticles on oxide supports, Appl. Catal. B Environ. 81 (2008) 225−235.
[23] W. Zhang, L. Li, Y. Du, X. Wang, P. Yang, Gold/platinum bimetallic core/shell nanoparticles stabilized by a fréchet-type dendrimer: preparation and catalytic hydrogenations of phenylaldehydes and nitrobenzenes, Catal. Lett. 127 (2009) 429−436.
[24] E.A. Karakhanov, A.L. Maximov, A.V. Zolotukhina, N. Yatmanova, E. Rosenberg, Alkyne hydrogenation using Pd-Ag hybrid nanocatalysts in surface-immobilized dendrimers, Appl. Organomet. Chem. 29 (2015) 777−784.
[25] P. Hohenberg, W. Kohn, Inhomogeneous electron gas, Phys. Rev. 136 (1964) B864−B871.
[26] W. Kohn, L.J. Sham, Self-consistent equations including exchange and correlation effects, Phys. Rev. 140 (1965) A1133−A1138.
[27] G. Kresse, J. Hafner, Ab initio molecular dynamics for liquid metals, Phys. Rev. B 47 (1993) 558−561.
[28] G. Kresse, J. Furthmüller, Efficient iterative schemes for ab initio total-energy calculations using a plane-wave basis set, Phys. Rev. B 54 (1996) 11169−11186.
[29] P.E. Blöchl, Projector augmented-wave method, Phys. Rev. B 50 (1994) 17953−17979.
[30] J.P. Perdew, K. Burke, M. Ernzerhof, Generalized gradient approximation made simple, Phys. Rev. Lett. 78 (1997), 1396−1396.
[31] M.J. Frisch, G.W. Trucks, H.B. Schlegel, G.E. Scuseria, M.A. Robb, J.R. Cheeseman, G. Scalmani, V. Barone, B. Mennucci, G.A. Petersson, H. Nakatsuji, M. Caricato, X. Li, H.P. Hratchian, A.F. Izmaylov, J. Bloino, G. Zheng, J.L. Sonnenberg, M. Hada, M. Ehara, K. Toyota, R. Fukuda, J. Hasegawa, M. Ishida, T. Nakajima, Y. Honda, O. Kitao, H. Nakai, T. Vreven, J.A. Montgomery Jr., J.E. Peralta, F. Ogliaro, M. Bearpark, J.J. Heyd, E. Brothers, K.N. Kudin, V.N. Staroverov, R. Kobayashi, J. Normand, K. Raghavachari, A. Rendell, J.C. Burant, S.S. Iyengar, J. Tomasi, M. Cossi, N. Rega, J.M. Millam, M. Klene, J.E. Knox, J.B. Cross, V. Bakken, C. Adamo, J. Jaramillo, R. Gomperts, R.E. Stratmann, O. Yazyev, A.J. Austin, R. Cammi, C. Pomelli, J.W. Ochterski, R.L. Martin, K. Morokuma, V.G. Zakrzewski, G.A. Voth, P. Salvador, J.J. Dannenberg, S. Dapprich, A.D. Daniels, Farkas, J.B. Foresman, J.V. Ortiz, J. Cioslowski, D.J. Fox, Gaussian 09 Revision A.1, 2009, Gaussian Inc., Wallingford CT, 2009.
[32] J.P. Perdew, Y. Wang, Accurate and simple analytic representation of the electron-gas correlation energy, Phys. Rev. B 45 (1992) 13244−13249.
[33] K.A. Peterson, Systematically convergent basis sets with relativistic pseudopotentials. I. Correlation consistent basis sets for the post-d group 13-15 elements, J. Chem. Phys. 119 (2003) 11099−11112.
[34] P.V. Nhat, N.T. Si, M.T. Nguyen, Elucidation of the molecular and electronic structures of some magic silver clusters Ag_n (n = 8, 18, 20), J. Mol. Model. 24 (2018) 209.
[35] M. Chen, J.E. Dyer, K. Li, D.A. Dixon, Prediction of structures and atomization energies of small silver clusters, $(Ag)_n$, n < 100, J. Phys. Chem. A 117 (2013) 8298−8313.
[36] P.L. Rodríguez-Kessler, A.R. Rodríguez-Domínguez, Size and structure effects of Pt_N (N = 12−13) clusters for the oxygen reduction reaction: first-principles calculations, J. Chem. Phys. 143 (2015) 184312.
[37] M.N. Huda, M.K. Niranjan, B.R. Sahu, L. Kleinman, Effect of spin-orbit coupling on small platinum nanoclusters, Phys. Rev., A 73 (2006), 053201.
[38] A. Grushow, K.M. Ervin, Ligand and metal binding energies in platinum carbonyl cluster Anions: collision-induced dissociation of $Pt_m^−$ and $Pt_m(CO)_n^−$, J. Chem. Phys. 106 (1997) 9580−9593.
[39] P. Błoński, J. Hafner, Geometric and magnetic properties of Pt clusters supported on graphene: relativistic density-functional calculations, J. Chem. Phys. 134 (2011) 154705.
[40] A. Sebetci, New minima for the Pt_8 cluster, Comput. Mater. Sci. 78 (2013) 9−11.
[41] A.S. Chaves, G.G. Rondina, M.J. Piotrowski, P. Tereshchuk, J.L.F. Da Silva, The role of charge states in the atomic structure of cu_n and Pt_n (n = 2−14 atoms) clusters: a DFT investigation, J. Phys. Chem. A 118 (2014) 10813−10821.
[42] V. Kumar, Y. Kawazoe, Evolution of atomic and electronic structure of Pt clusters: planar, layered, pyramidal, cage, cubic, and octahedral growth, Phys. Rev. B 77 (2008) 205418.
[43] F. Aguilera-Granja, R.C. Longo, L.J. Gallego, A. Vega, Structural and magnetic properties of $X_{12}Y$ (X, Y=Fe, Co, Ni, Ru, Rh, Pd, and Pt) nanoalloys, J. Chem. Phys. 132 (2010) 184507.
[44] A.M. Köster, P. Calaminici, E. Orgaz, D.R. Roy, J.U. Reveles, S.N. Khanna, On the ground state of Pd_{13}, J. Am. Chem. Soc. 133 (2011) 12192−12196.
[45] P. Rodríguez-Kessler, J. Ricardo-Chávez, Structures of FePt clusters and their interactions with the O_2 molecule, Chem. Phys. Lett. 622 (2015) 34−41.
[46] J.S. Shpilman, A. Friedman, N. Zion, N. Levy, D.T. Major, L. Elbaz, Combined experimental and theoretical study of cobalt corroles as catalysts for oxygen reduction reaction, J. Phys. Chem. C 123 (2019) 30129−30136.
[47] R. Parr, P. Chattaraj, Principle of maximum hardness, J. Am. Chem. Soc. 113 (1991) 1854−1855.
[48] R. Pearson, Recent advances in the concept of hard and soft acids and bases, J. Chem. Educ. 64 (1987) 561−567.
[49] P.L. Rodríguez-Kessler, A.R. Rodríguez-Domínguez, Stability of Ni clusters and the adsorption of CH_4: first-principles calculations, J. Phys. Chem. C 119 (2015) 12378−12384.
[50] R.V. de Amorim, K.E.A. Batista, G.R. Nagurniak, R.P. Orenha, R.L.T. Parreira, M.J. Piotrowski, CO, NO, and SO adsorption on Ni nanoclusters: a DFT investigation, Dalton Trans. 49 (2020) 6407−6417.

[51] J.H. Stenlid, T. Brinck, Extending the σ-hole concept to metals: an electrostatic interpretation of the effects of nanostructure in gold and platinum catalysis, J. Am. Chem. Soc. 139 (2017) 11012−11015.

[52] K. Cheng, D. He, T. Peng, H. Lv, M. Pan, S. Mu, Porous graphene supported Pt catalysts for proton exchange membrane fuel cells, Electrochim. Acta 132 (2014) 356−363.

[53] Y. Yang, P. Cheng, S. Huang, Unraveling the roles of iron in stabilizing the defective graphene-supported PtFe bimetallic nanoparticles, J. Alloys Compd. 688 (2016) 1172−1180.

[54] K. Jansson, R. Scullman, Optical absorption spectra of PtO and Pt$_2$ in rare-gas matrices, J. Mol. Spectrosc. 61 (1976) 299−312.

[55] N.B. Singh, U. Sarkar, Structure, vibrational, and optical properties of platinum cluster: a density functional theory approach, J. Mol. Model. 20 (2014) 2537.